Utilizing Benign Oxidants for Selective Aerobic Oxidations using Heterogenized Platinum Nanoparticle Catalysts

Christopher S. Hinde,[a] Arran M. Gill,[a] Peter P. Wells,[b,c] T. S. Andy Hor,[d,e] and Robert Raja*[a]

Abstract: By using platinum nanoparticle catalysts that are generated *in situ* by extrusion from a porous copper chlorophosphate framework, the role of oxidants in the selective oxidation of benzyl alcohol to benzaldehyde was evaluated, with a view to establishing structure-property relationships. With a detailed study of the kinetic properties of the oxidation reaction, it has been determined that the aerobic oxidation pathways progress with lower levels of product selectivity and higher activation energies (72.4 kJ/mol) than the peroxide-based ones (23.6 kJ/mol); affording valuable insights in the design of solid catalysts for selective oxidation reactions. Furthermore, through the use of X-ray absorption spectroscopy, the effect of calcination temperature on the degree of extrusion and its influence on nanoparticle formation have been evaluated, leading to the establishment of structure-activity correlations between the observed activation energies and the proportion of nanoparticle species generated .

Oxidation reactions are ubiquitous in the pharmaceutical and fine-chemical industries, and are fundamentally important to introducing oxygen rich functional groups to organic molecules. For example, aldehyde and ester containing molecules are heavily employed as flavouring and fragrance agents due to their volatility and distinctly aromatic nature that are often pleasing to smell and taste.[1] Benzaldehyde is a key component for most almond-based flavourings, although it finds other uses as precursors for plastic additives and as a pharmaceutical intermediate toward antibiotic drugs such as chloramphenicol and ampicillin, as well as stimulants like ephedrine.[2] Industrially, it is synthesized by the hydrolysis of benzal chloride, however the dehydrogenative oxidation of benzyl alcohol is a viable chloride free and environmentally benign alternative.[2]

Traditionally, industrial oxidation reactions are based on the use of stoichiometric quantities of inorganic metal-based oxidizing agents such as MnO_2 or CrO_3, or harsh mineral acids like H_2SO_4 and HNO_3, which result in hazardous, corrosive and toxic operating conditions as well as leading to the generation of large quantities of polluting waste by-products.[3] Due to the heightened socio-economic demand for the chemical and related industries to reduce their negative impact on the environment, there is a significant drive to find alternative economic and sustainable oxidation reagents and synthetic protocols.[3] The abundance of molecular oxygen, its high atom-economy in oxidation reactions, low costs and mild reaction conditions make it an appealing candidate as an oxidant,[4] although high-pressure and relatively high reaction temperatures are often required, owing to the gaseous nature of the reaction. Similarly, simple peroxides such as H_2O_2 and *tert*-butyl hydroperoxide (TBHP), are often considered as alternative green oxidants.[4] Although, this often leads to the generation of larger quantities of by-products in comparison with molecular oxygen, they are slightly more reactive due to the lower bond dissociation energy (BDE) of the single O-O bond (49.7 kcal/mol for H_2O_2 and 45.0 kcal/mol for TBHP)[5] compared with O=O (118 kcal/mol),[6] with the added potential to operate under comparatively mild conditions. Nonetheless, suitable catalysts are often still required to activate the oxidants in order to achieve respectable activity and selectivity within reasonable reaction conditions.

In recent years, supported noble metal nanoparticle (NP) catalysts have shown great promise in the activation of both molecular oxygen[7] and simple peroxides[8] to achieve selective oxidation of alcohols, and more recently, activation of C-H bonds in hydrocarbon substrates such as toluene.[8c, 9] We recently reported a new method for the synthesis of highly active, uniform and site-isolated metal NPs *in situ,* by extrusion of chlorometallate precursor anions from the 1D channels of a porous copper chlorophosphate (CuCIP) framework, for the activation of O_2 and base-free oxidation of alcohols.[10] It was demonstrated that calcination of the as-synthesised materials in air could generate fractions of supported, active NP catalysts for the aerobic oxidations, with the Pt/CuCIP showing the best activity and selectivity. A significant challenge in the development of sustainable oxidation catalysts relies on a detailed understanding of the nature of the active sites at a molecular level, which requires a multidisciplinary design-application approach, drawing on strengths of materials chemistry and spectroscopic characterization. By gaining in-depth knowledge of the local structural environment of the active centres within catalytic nanostructures (through x-ray absorption spectroscopy), precise structure-property correlations can be established, with a view to adopting a more generalized approach for the predictive design of single-site heterogeneous catalysts in industrially-significant, sustainable oxidation reactions.

In this study, we evaluate the propensity of Pt/CuCIP catalysts toward the activation of O_2 and TBHP for the selective

[a]   C. S. Hinde, A. M. Gill and Dr. R. Raja
        University of Southampton
        Southampton, SO17 1BJ, UK.
        E-mail: R.Raja@soton.ac.uk
[b]   Dr. P. P. Wells
        UK Catalysis Hub
        Oxon, OX11 0FA, UK.
[c]   University College London
        London, WC1H 0AJ, UK.
[d]   Prof. T. S. A. Hor
        Institute of Materials Science and Engineering (IMRE), Agency for Science, Technology & Research (A*STAR), 3 Research Link, Singapore, 117602.
[e]   Department of Chemistry, National University of Singapore, 3 Science Drive 3,
        Singapore, 117543.

        Supporting information for this article is given via a link at the end of the document.

oxidation of benzyl alcohol to benzaldehyde in batch conditions. Through detailed kinetic studies, activation energies are calculated to compare the ability of the catalysts to activate both oxidants, with the selectivity profiles critically evaluated to establish the merits of each process. In addition, the effect of calcination temperature on the activation of the catalyst will be studied, to investigate its influence on the resulting catalytic properties, in order to facilitate structure-property relationships.
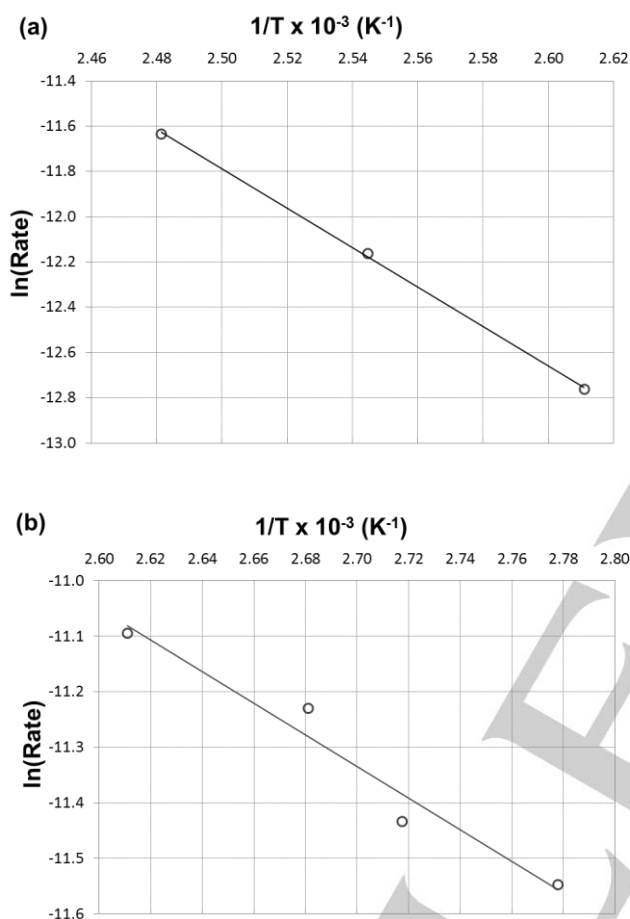

Figure 1. Arrhenius plots for the (a) aerobic and (b) TBHP oxidations of benzyl alcohol with calcined (500 °C, 2 h) Pt/CuCIP catalyst. Conversion vs. time plots and reaction conditions are given in (a); Figure SI-1 and (b); Figure SI-2

A kinetic study was performed for the aerobic oxidation of benzyl alcohol by analysis of the conversion rates at different reaction temperatures. The reaction profile of the Pt catalyst was zero-order with respect to the conversion of benzyl alcohol, showing little dependence of the substrate concentration on the rate of reaction (Figure SI-4). Furthermore, the kinetic data was used to construct an Arrhenius plot (Figure 1a.) to calculate the activation energy for this reaction at 72.4 kJ/mol. Interestingly, it was noted in our earlier work[10] that different reaction rates and selectivity profiles were observed for equivalent Au and Pd/CuCIP catalysts. These changes in the observed rates could

however, be due to the differing extents of extrusion between each material which is now thought to be a consequence of the activation temperatures employed.

Investigation into the kinetics of the TBHP oxidation of benzyl alcohol using the same calcined Pt/CuCIP (Figure 1b.), revealed an activation energy of 23.6 kJ/mol under identical conditions and concentrations employed for the aerobic oxidation. This is also in agreement with analogous supported NP materials for peroxide oxidation of benzyl alcohol at 38[11] and 20[12] kJ/mol, whilst surpassing the values obtained for transition-metal catalysts based on Mo and W at 84 and 96 kJ/mol respectively.[13] The lower activation energy of the peroxide based oxidation is not surprising; given the lower BDE of TBHP juxtaposed with O_2, and as reflected, in the activity of the catalyst at temperatures lower than 100 °C. With blank reactions not yielding appreciable conversions (Table SI-1), it is clear that the Pt/CuCIP catalyst is able to effectively activate both TBHP and O_2 as oxidants.

It is interesting to note the deviation from zero-order kinetics, as observed for the O_2 system, after low levels of conversion for the TBHP oxidation. The rate of benzyl alcohol oxidation with TBHP reduces over time and thus indicates a dependence on the concentrations of the benzyl alcohol and/or TBHP in the reaction (Figure SI-5). In contrast, the selectivity of the TBHP oxidation is maintained at > 99 % throughout the course of the reaction, whereas benzoic acid is observed, as a significant by-product, in the aerobic oxidation (Figure SI-4). The higher temperature and pressure required for the O_2 oxidation could be responsible for the formation of the benzoic acid over-oxidation product.
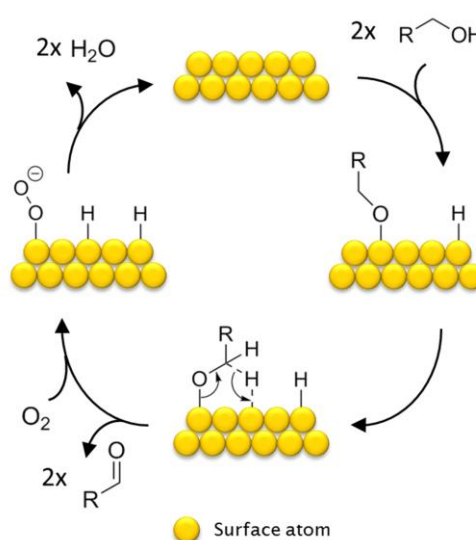
Figure 2. Mechanism for aerobic oxidation of an alcohol to an aldehyde on a metallic NP surface in organic media

For Pt NPs, it is generally accepted that the mechanism of action varies between aqueous and organic media,[14] whereby water facilitates radical-type processes[15] and organic media

promotes heterolytic mechanisms, as with Au NP systems. Through extensive studies on Au NPs, it has been determined that the adsorption of O_2 or peroxides can form activated surface-adsorbed superoxide or surface-peroxide species that can facilitate the dehydrogenation process (Figure 2.).[16] The subsequent adsorption of the alcohol to form an adsorbed surface-alcoholate species then occurs. Abstraction of the β hydride to the surface of the metal generates the desorbed aldehyde species, with the surface hydrides reacting with the activated surface peroxo-species to form water and regenerate sites for adsorption and further catalytic cycles.[17] It is likely that similar mechanisms operate also for Pt NP systems in organic solvents, including these Pt/CuClP catalysts.

Before probing the catalytic properties of these materials an ideal candidate was to be selected and thus, a range of catalysts activated under different calcination temperatures (200 – 600 °C) were subjected to X-ray absorption fine structure (XAFS) analysis and herein contrasted, in order to determine whether the extent of extrusion is indeed, a function of temperature. The first shell extended X-ray absorption fine structure (EXAFS) fitting parameters are shown in Table SI-2, along with the magnitude and imaginary components of the k^3 weighted Fourier transform data and their corresponding fits in Figure SI-5. The EXAFS data shows a mild increase in Pt-Pt coordination numbers (0.8 – 1.2) and a respective decrease in Pt-Cl coordination (4.5 – 3.7), suggesting a minor relation between the extent of NP formation and the calcination temperature. Despite the percentage errors, particularly with the lower coordination numbers being larger than desired, the trend is supported by catalytic comparisons with TBHP. The percentage conversions shown in Table 1 display a significant and progressive increase with catalyst calcination temperatures, which provide a clear indication that the activation temperature is directly related to NP formation (via extrusion), and that this has a direct influence on the catalytic activity of these materials.

Table 1. Conversions and product distributions of Pt/CuClP catalysts activated under increasing calcination temperature

Calcination Temperature	Conversion	Benzaldehyde (%)	Benzoic Acid (%)	Benzyl Benzoate (%)
200 °C	14.9	> 99.0	0.0	0.0
400 °C	21.8	> 99.0	0.0	0.0
500 °C	38.6	97.8	2.2	0.0
600 °C	86.9	65.4	34.3	0.3

Reaction conditions: 65 °C, 6 h, benzyl alcohol (27.7 mmol), substrate to oxidant (TBHP) mole ratio = 1.00:1.15, diethylene glycol dimethyl ether (11.2 mmol) and catalyst, calcined for 2 h (50 mg)

Nevertheless, it has been observed that when the calcination temperature exceeds 500 °C, the selectivity of the catalyst drastically diminishes. In addition, it was previously noted[18] that these materials can become victim to thermal degradation at temperatures in excess of 600 °C, and indeed, inconsistencies within the powder X-ray diffraction patterns (PXRD) of these materials are observed at such elevated temperatures (Figure SI-6). Thus, as a result of these observations, all kinetic work conducted herein with the Pt/CuClP catalysts were subject to activation via calcination at 500 °C, and with optimized oxidant to substrate ratios for maximizing the reaction selectivity towards benzaldehyde.

With the EXAFS fitting parameters presented in Table 2. taken into consideration, the Pt-Cl and Pt-Pt coordination numbers clearly show that only a fraction of the chlorometallate anions have been extruded to form metallic NPs on the surface of the materials, which is consistent with our earlier microscopy studies.[10] As the rate of reaction is correlated with available active sites on the NP surface and the activation energy directly associated with the rates of reaction; it is noteworthy that the activation energies observed in our (partially) activated catalysts compete with those reported in the literature with analogous materials.[11,12] Therefore, with an established method for complete extrusion, it should be possible to significantly improve on these values. Further analysis of activation parameters on structural properties and extent of extrusion is currently ongoing.

Table 2. EXAFS fitting parameters for the Pt/CuClP material calcined for 2 h at 500 °C

Abs Sc	N	R / Å	$2\sigma^2$ / Å^2	E_f / eV	R_{factor}
Pt – Cl	4.4 (2)	2.320 (6)	0.0026 (4)	9 (1)	0.013
Pt – Pt	1.4 (5)	2.78 (2)	0.004 (2)		

Fitting parameters: S_0^2 = 0.91 as deduced by Pt foil standard; fit range 3<k<12.5, 1<R<3; # of independent points = 12

In summary, a combination of spectroscopic and catalytic approaches have revealed that activation conditions play a crucial role in controlling the morphology, size and local structural environment of Pt nanoparticle catalysts, which are generated by a one-step extrusion process. Spectroscopic and kinetic analysis further illustrate that the presence of well-defined and isolated nanoparticles is fundamental to activating molecular oxygen, for the aerobic oxidation of benzylic alcohols, and the ensuing structure-property correlations pave the way for the predictive design of solid catalysts. Comparison of activation energies showed a higher value for aerobic oxidation at 72.4 kJ/mol, compared with 23.6 kJ/mol for the TBHP oxidation. The aerobic oxidation sustained high rates of conversion with zero-order kinetics and thus negligible influence of substrate concentrations on reaction rates. On the other hand, the reaction had a reduced selectivity, with benzoic acid formed as a significant by-product, due to the high temperature and pressures required. Oxidation with TBHP maintained a high level of selectivity with negligible quantities of by-products formed. This was, however, limited by substrate concentration effects that resulted in heavily reduced rates of reaction after 4-5 hours. The Pt/CuClP NP catalyst was successful in activating both of these green alternative oxidants, bestowing unique advantages to each process, thereby affording considerable scope for the further exploitation of these catalysts and design strategy. Given the above, the oxidant can be opportunistically selected depending on whether selectivity for the aldehyde or acid is

required, notwithstanding the requirement to maintain high reaction rates.

This general approach in evaluating oxidation potentials of nanoparticle-based materials, through the integration of detailed structural characterization and analysis of chemical environments, allows for precise molecular engineering of heterogeneous single-site nanocatalysts with applications in a wide-array of organic processes. As hybrid nanomaterials have also been utilized elsewhere in hydrogenation and C-C coupling reactions,[19] as well as for sensors,[20] therapeutic agents and other bio-related applications,[21] it is possible to envisage similar approaches to achieve fundamental understanding of materials for the development of new technologies.

[1] K.-G. Fahlbusch, F.-J. Hammerschmidt, J. Panten, W. Pickenhagen, D. Schatkowski, K. Bauer, D. Garbe, H. Surburg, in *Ullmann's Encyclopedia of Industrial Chemistry, Vol. 15*, 7th ed., Wiley-VCH Verlag GmbH & Co. KGaA, **2003**, pp. 73-198.

[2] (a) F. Brühne, E. Wright, in *Ullmann's Encyclopedia of Industrial Chemistry, Vol. 5*, 7th ed., Wiley-VCH Verlag GmbH & Co. KGaA, **2011**, pp. 223-235; (b) J. L. Opgrande, E. Brown, M. Hesser, J. Andrews, in *Kirk-Othmer Encyclopedia of Chemical Technology*, John Wiley & Sons, Inc., **2003**.

[3] (a) G. Franz, R. A. Sheldon, in *Ullmann's Encyclopedia of Industrial Chemistry, Vol. 25*, 7th ed., Wiley-VCH Verlag GmbH & Co. KGaA, **2000**, pp. 543-600; (b) I. W. C. E. Arends, R. A. Sheldon, in *Modern Oxidation Methods* (Ed.: J.-E. Bäckvall), Wiley-VCH Verlag GmbH & Co. KGaA, Weinheim, **2004**, pp. 83-118.

[4] R. A. Sheldon, *Chem. Soc. Rev.* **2012**, *41*, 1437-1451.

[5] E. P. Clifford, P. G. Wenthold, R. Gareyev, W. C. Lineberger, C. H. DePuy, V. M. Bierbaum, G. B. Ellison, *The Journal of Chemical Physics* **1998**, *109*, 10293-10310.

[6] V. I. Vedeneyev, *Bond Energies, Ionization Potentials and Electron Affinities*, Hodder & Stoughton Educational, London, **1966**.

[7] (a) Y.-F. Huang, M. Zhang, L.-B. Zhao, J.-M. Feng, D.-Y. Wu, B. Ren, Z.-Q. Tian, *Angew. Chem., Int. Ed.* **2014**, *53*, 2353-2357; (b) J. Gong, C. B. Mullins, *Acc. Chem. Res.* **2009**, *42*, 1063-1073; (c) D. Widmann, R. J. Behm, *Acc. Chem. Res.* **2014**, *47*, 740-749; (d) D. I. Enache, J. K. Edwards, P. Landon, B. Solsona-Espriu, A. F. Carley, A. A. Herzing, M. Watanabe, C. J. Kiely, D. W. Knight, G. J. Hutchings, *Science* **2006**, *311*, 362-365.

[8] (a) A. Quintanilla, S. García-Rodríguez, C. M. Domínguez, S. Blasco, J. A. Casas, J. J. Rodriguez, *Appl. Catal., B* **2012**, *111–112*, 81-89; (b) J. Ni, W.-J. Yu, L. He, H. Sun, Y. Cao, H.-Y. He, K.-N. Fan, *Green Chem.* **2009**, *11*, 756-759; (c) V. Peneau, Q. He, G. Shaw, S. A. Kondrat, T. E. Davies, P. Miedziak, M. Forde, N. Dimitratos, C. J. Kiely, G. J. Hutchings, *Phys. Chem. Chem. Phys.* **2013**, *15*, 10636-10644.

[9] (a) Y. T. Lai, T. C. Chen, Y. K. Lan, B. S. Chen, J. H. You, C. M. Yang, N. C. Lai, J. H. Wu, C. S. Chen, *ACS Catal.* **2014**, *4*, 3824-3836; (b) L. Kesavan, R. Tiruvalam, M. H. A. Rahim, M. I. bin Saiman, D. I. Enache, R. L. Jenkins, N. Dimitratos, J. A. Lopez-Sanchez, S. H. Taylor, D. W. Knight, C. J. Kiely, G. J. Hutchings, *Science* **2011**, *331*, 195-199; (c) M. I. bin Saiman, G. L. Brett, R. Tiruvalam, M. M. Forde, K. Sharples, A. Thetford, R. L. Jenkins, N. Dimitratos, J. A. Lopez-Sanchez, D. M. Murphy, D. Bethell, D. J. Willock, S. H. Taylor, D. W. Knight, C. J. Kiely, G. J. Hutchings, *Angew. Chem., Int. Ed.* **2012**, *51*, 5981-5985; (d) S. Ghosh, S. S. Acharyya, D. Tripathi, R. Bal, *J. Mater. Chem. A* **2014**, *2*, 15726-15733.

[10] C. S. Hinde, S. Van Aswegen, G. Collins, J. D. Holmes, T. S. A. Hor, R. Raja, *Dalton Trans.* **2013**, *42*, 12600-12605.

[11] G. Zhan, Y. Hong, F. Lu, A.-R. Ibrahim, M. Du, D. Sun, J. Huang, Q. Li, J. Li, *J. Mol. Catal. A: Chem.* **2013**, *366*, 215-221.

[12] A. Mehri, H. Kochkar, G. Berhault, D. F. Cómbita Merchán, T. Blasco, *Mater. Chem. Phys.* **2015**, *149–150*, 59-68.

[13] M. P. Chaudhari, S. B. Sawant, *Chem. Eng. J.* **2005**, *106*, 111-118.

[14] N. Dimitratos, A. Villa, D. Wang, F. Porta, D. Su, L. Prati, *J. Catal.* **2006**, *244*, 113-121.

[15] (a) Y. Hong, X. Yan, X. Liao, R. Li, S. Xu, L. Xiao, J. Fan, *Chem. Commun.* **2014**, *50*, 9679-9682; (b) T. Wang, H. Shou, Y. Kou, H. Liu, *Green Chem.* **2009**, *11*, 562-568.

[16] A. Abad, A. Corma, H. García, *Chem. Eur. J.* **2008**, *14*, 212-222.

[17] (a) H. Tsunoyama, H. Sakurai, Y. Negishi, T. Tsukuda, *J. Am. Chem. Soc.* **2005**, *127*, 9374-9375; (b) P. Fristrup, L. Johansen, C. Christensen, *Catal. Lett.* **2008**, *120*, 184-190.

[18] E. R. Williams, R. M. Leithall, R. Raja, M. T. Weller, *Chem. Commun.* **2013**, *49*, 249-251.

[19] (a) G. Collins, M. Schmidt, C. O'Dwyer, J. D. Holmes, G. P. McGlacken, *Angew. Chem., Int. Ed.* **2014**, *53*, 4142-4145; (b) Z. Wang, K.-D. Kim, C. Zhou, M. Chen, N. Maeda, Z. Liu, J. Shi, A. Baiker, M. Hunger, J. Huang, *Catal. Sci. Technol.* **2015**, *5*, 2788-2797.

[20] J. Xie, Y. Zheng, J. Y. Ying, *Chem. Commun.* **2010**, *46*, 961-963.

[21] B. H. Kim, M. J. Hackett, J. Park, T. Hyeon, *Chem. Mater.* **2013**, *26*, 59-71.

Entry for the Table of Contents (Please choose one layout)

Layout 1:

COMMUNICATION

A versatile design strategy for the *in situ* generation of well-defined platinum nanoparticles, which are heterogenized by anion extrusion within porous framework architectures, affords dextrous control for tuning the local structural environment of the active site, in enabling industrially-significant, sustainable catalytic oxidations.
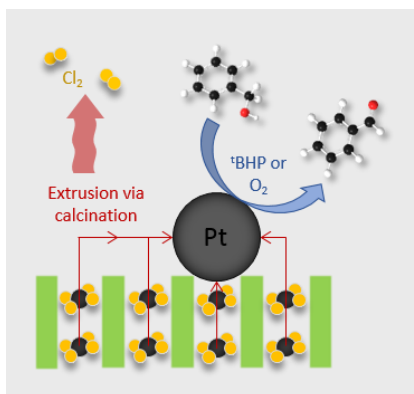
Christopher S Hinde, Arran M. Gill, Peter P. Wells, T.S. Andy Hor and Robert Raja*

Page No. – Page No.

Utilizing Benign Oxidants for Selective Aerobic Oxidations using Heterogenized Platinum Nanoparticle Catalysts

Contents

1.   Experimental section

Synthesis of 7 wt % Pt/CuCIP: Copper(II) fluoride (1.150 mmol), 85 wt.% orthophosphoric acid (2.922 mmol), 50 wt.% RbOH (2.037 mmol), RbCl (2.316 mmol) and K_2PtCl_4 (0.124 mmol) were mixed in the PTFE liner of a custom-made 23 cm^3 hydrothermal vessel. The vessel was sealed and heated to 448 K for 2 days. Products formed as brilliant green cuboid crystals for the Pt copper chlorophosphate material. Materials were further activated by calcination (air, 2 h) at designated temperatures to generate the active NP catalysts. After calcination, the materials appeared a darker khaki-green.

Catalytic reactions with O_2: High-pressure reactions were carried out in a 75 cm^3 PTFE lined, stainless-steel Parr batch reactor. The reactor was charged with benzyl alcohol (9.247 mmol), diethylene glycol dimethyl ether (6.335 mmol) as an internal standard, *t*-butanol (30 mL) as a solvent and catalyst (50 mg). The reactor was pressurized with ≈20 bar of dry air (yielding an oxidant to substrate molar ratio of 1:0.85), stirred and heated for the required amount of time. Small aliquots of the reaction mixture were taken carefully periodically for GC analysis. Samples were analyzed by GC (PerkinElmer, Clarus 480) using an Elite-5 column equipped with a flame ionization detector (FID). Products were identified against authenticated standards and quantified by calibration to obtain response factors (RF) against the known internal standard.

Catalytic reactions with TBHP: A standard reflux setup was charged with benzyl alcohol (4.624 mmol), diethylene glycol dimethyl ether (2.981 mmol) as an internal standard, *t*-butanol (15 mL) as a solvent and catalyst (25 mg). TBHP (11.0 mmol in decane) was added lastly yielding a substrate to oxidant molar ratio of 1:0.85. The reaction was stirred and heated for the required amount of time. Small aliquots of the reaction mixture were taken carefully periodically for GC analysis, as above.

XAFS: Pt L_3-edge XAFS measurements were carried out on the B18 beamline at the Diamond Light Source, Didcot, UK. Measurements were performed using a QEXAFS set-up with a fast-scanning Si (111) double crystal monochromator. The normal time resolution of the spectra reported herein was 1 min/spectrum (k_{max} = 16), on average six scans were acquired to improve the signal to noise level of the data. All samples were diluted with cellulose and pressed into pellets to optimize the effective edge-step of the XAFS data and measured in transmission mode using ion chamber detectors. All transmission XAFS spectra were acquired concurrently with the appropriate reference foil placed between I_t and I_{ref}. XAS data processing and EXAFS analysis were performed using IFEFFIT with the Horae package (Athena and Artemis).[1,2] The amplitude reduction factor, s_o^2, was derived from EXAFS data analysis of known compounds, and used as a fixed input parameter.

PXRD: Data were collected on a Bruker D2 Phaser in theta-theta geometry using Cu (Kα1/Kα2) radiation and a Ni Kβ filter (detector side). Additional beam optics and settings: primary and secondary axial Soller slits (2.5°), fixed 0.6mm divergence slit, 1mm anti-scatter-screen, Detector: 1D LYNXEYE with a 5° window, Generator: 30kV, 10mA.

2.   Kinetic plots for aerobic oxidation of benzyl alcohol
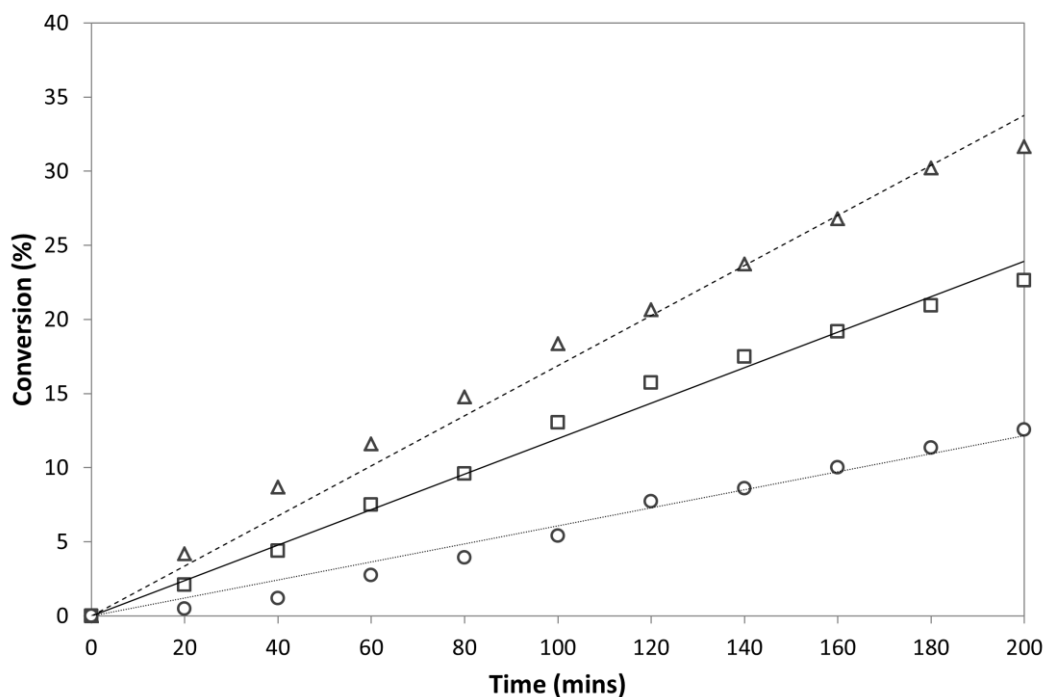
Figure SI-1 – Kinetic plot showing conversion of benzyl alcohol by aerobic oxidation with the calcined (500 °C, 2 h) Pt/CuClP at 110 °C (circles), 120 °C (squares) and 130 °C (triangles). Reaction conditions: benzyl alcohol (9.247 mmol), catalyst (50 mg), diglyme as internal standard (6.335 mmol), *t*-butanol (30 mL), air (20 bar), oxidant to substrate molar ratio of 1:0.85
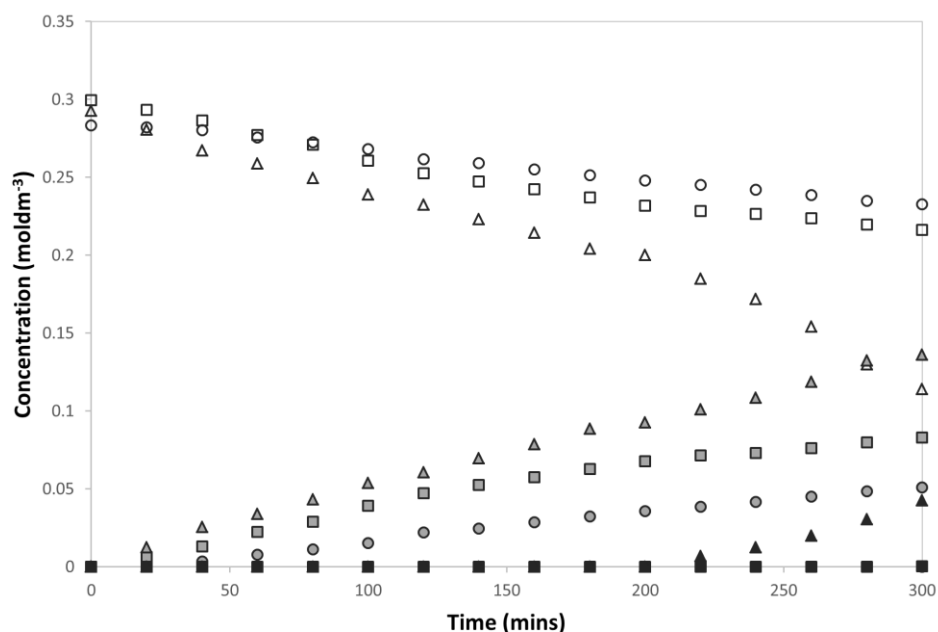
3.   Kinetic Plots for TBHP oxidation of benzyl alcohol
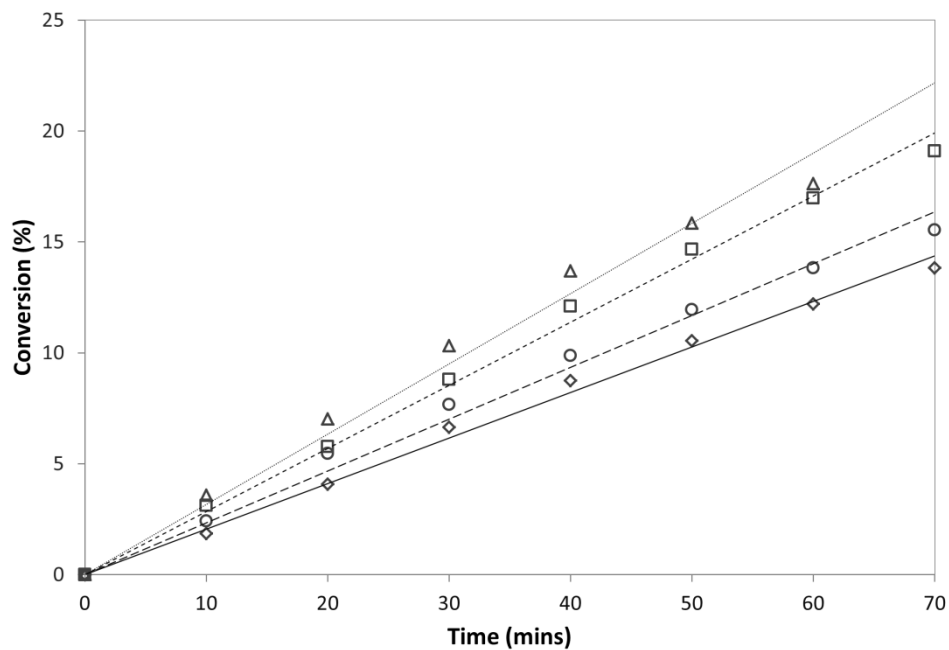
Figure SI-2 – Kinetic plot showing conversion of benzyl alcohol by TBHP oxidation with the calcined (500 °C, 2 h) Pt/CuClP at 87 °C (diamonds) 95 °C (circles), 100 °C (squares) and 110 °C (triangles). Reaction conditions: benzyl alcohol (4.624 mmol), catalyst (25 mg), diglyme as internal standard (2.981 mmol), *t*-butanol (15 mL), TBHP (11.0 mmol in decane), oxidant to substrate molar ratio of 1:0.85
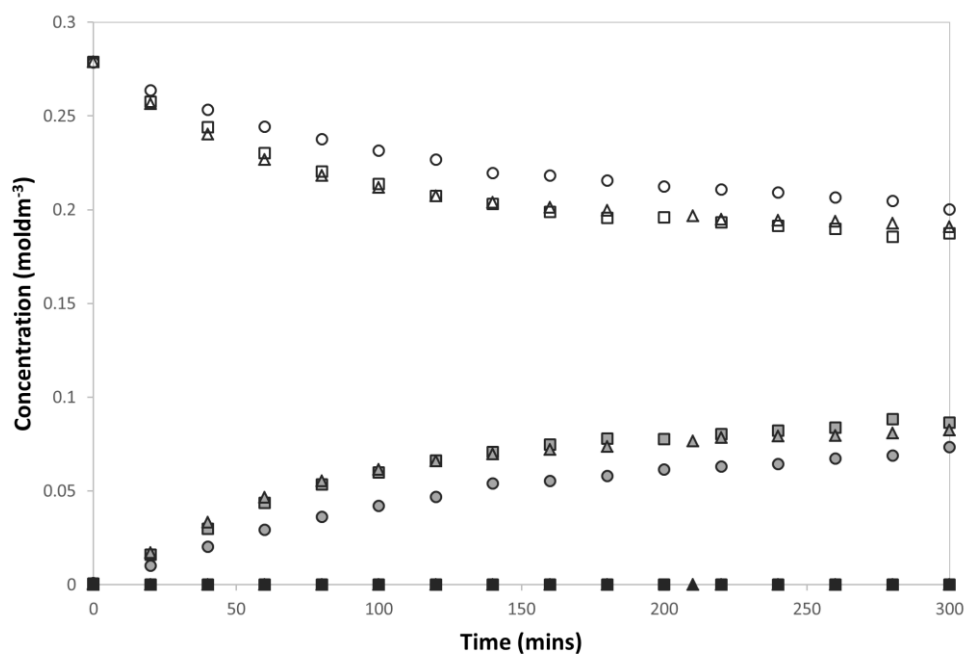
4.   Concentration profiles for aerobic oxidation of benzyl alcohol

Figure SI-3 – Plot showing the change in benzyl alcohol (white fill), benzaldehyde (grey fill) and benzoic acid (black fill) concentration with time in the aerobic oxidation of benzyl alcohol with the calcined (500 °C, 2 h) Pt/CuClP at 110 °C (circles), 120 °C (squares) and 130 °C (triangles). Reaction conditions: benzyl alcohol (9.247 mmol), catalyst (50 mg), diglyme as internal standard (6.335 mmol), *t*-butanol (30 mL), air (20 bar), oxidant to substrate molar ratio of 1:0.85

## 5.   Concentration profiles for TBHP oxidation of benzyl alcohol

Figure SI-4 – Plot showing the change in benzyl alcohol (white fill), benzaldehyde (grey fill) and benzoic acid (black fill) concentration with time in the TBHP oxidation of benzyl alcohol with the calcined (500 °C, 2 h) Pt/CuClP at 86 °C (circles), 100 °C (squares) and 110 °C (triangles). Reaction conditions: benzyl alcohol (4.624 mmol), catalyst (25 mg), diglyme as internal standard (2.981 mmol), *t*-butanol (15 mL), TBHP (11.0 mmol in decane), oxidant to substrate molar ratio of 1:0.85

6. Additional catalysis data

Oxidant	Temperature / °C	Time / min	Conversion / %	Benzaldehyde Selectivity / %	Benzoic Acid Selectivity / %
Air[a]	130	300	8	>99	0
TBHP[b]	110	300	6	> 99	0

Table SI-1 – Full blank reaction results with corresponding conversions and selectivities at the quoted temperature and reaction time. Reaction conditions [a]: benzyl alcohol (9.247 mmol), diglyme as internal standard (6.335 mmol), *t*-butanol (30 mL), air (20 bar), oxidant to substrate molar ratio of 1:0.85. Reaction conditions [b]: benzyl alcohol (4.624 mmol), diglyme as internal standard (2.981 mmol), *t*-butanol (15 mL), TBHP (11.0 mmol in decane), oxidant to substrate molar ratio of 1:0.85

7. EXAFS data & fits
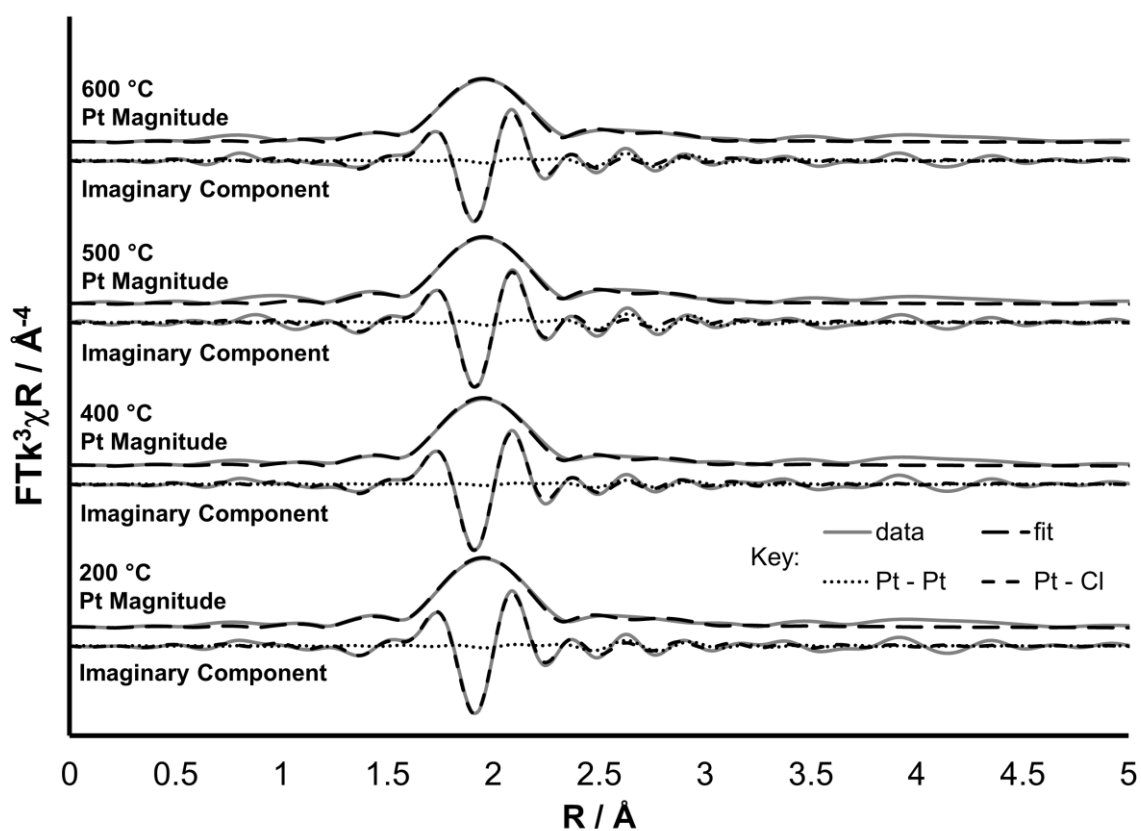
Figure SI-5 – Magnitude and imaginary component of the k^3 weighted Fourier transform for the EXAFS data of the Pt/CuClP materials calcined (2 h) under increasing activation temperature, ascending up the plot. Associated scattering paths are included for the imaginary component

7.   EXAFS fitting parameters

Sample	Abs Sc	N	R / Å	$2\sigma^2$ / Å^2	E_f / eV	R_{factor}
Pt/CuClP	Pt – Cl	4.5 (2)	2.320 (5)	0.0024 (3)	8.8 (9)	0.010
200 °C	Pt – Pt	0.8 (5)	2.77 (3)	0.004 (2)		
Pt/CuClP	Pt – Cl	5.0 (2)	2.319 (5)	0.0026 (3)	8.8 (9)	0.012
400 °C	Pt – Pt	0.8 (8)	2.78 (4)	0.004 (4)		
Pt/CuClP	Pt – Cl	4.4 (2)	2.320 (6)	0.0026 (4)	9 (1)	0.013
500 °C	Pt – Pt	1.4 (5)	2.78 (2)	0.004 (2)		
Pt/CuClP	Pt – Cl	3.7 (2)	2.317 (5)	0.0025 (3)	9.2 (9)	0.011
600 °C	Pt – Pt	1.2 (5)	2.78 (2)	0.005 (2)		

Table SI-2 – EXAFS fitting parameters of the Pt/CuClP materials calcined (2 h) under increasing activation temperature. S_0^2 = 0.91 as deduced by Pt foil standard; fit range 3<k<12.5, 1<R<3; # of independent points = 12

8.   Powder X-ray diffraction analysis
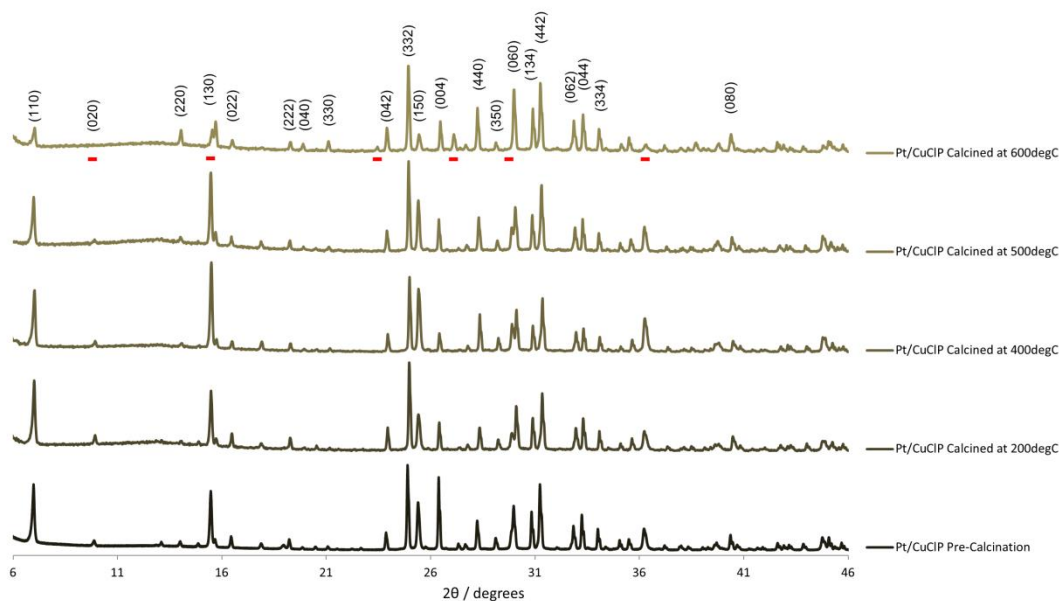
Figure SI-6 – Indexed PXRD patterns for the Pt/CuClP under increasing calcination temperature. Data shown of the un-calcined sample through 200, 400, 500 and 600 ^{o}C up the plot (all materials were calcined for 2 h). Changes in the PXRD pattern are observed when the material is calcined at 600 ^{o}C which have been highlighted with red markers

9.   Bibliography

[1]   M. Newville, *J. Synchrotron Radiat.* **2001**, *8*, 322–324.

[2]   B. Ravel, M. Newville, *J. Synchrotron Radiat.* **2005**, *12*, 537–541.